Korean J. Chem. Eng., 38(11), 2279-2285 (2021)
DOI: 10.1007/s11814-021-0874-5

pISSN: 0256-1115
eISSN: 1975-7220

Evaluation of elemental leaching behavior and morphological changes of steel slag in both acidic and basic conditions for carbon sequestration potential

Sujin Hong*, Ah-Hyung Alissa Park,***,****, and Youngjune Park*,†**

*School of Earth Sciences and Environmental Engineering, Gwangju Institute of Science and Technology (GIST), 123 Cheomdangwagi-ro, Buk-gu, Gwangju 61005, Korea
**Department of Earth and Environmental Engineering, Columbia University, 500 W. 120th St, New York, NY 10027, United States
***Lenfest Center for Sustainable Energy, The Earth Institute, Columbia University, 500 W. 120th St, New York, NY 10027, United States
****Department of Chemical Engineering, Columbia University, 500 W. 120th St, New York, NY 10027, United States
(*Received 10 May 2021 • Revised 13 June 2021 • Accepted 19 June 2021*)

Abstract−Carbon mineralization technology involves reactions between carbon dioxide (CO_2) and alkali earth metals such as calcium and/or magnesium to form thermodynamically stable solid carbonates (i.e., $CaCO_3$, and $MgCO_3$), and is currently being recognized as a promising method of both storing and utilizing CO_2. In particular, industrial solid wastes such as steelmaking slags (steel and iron slags) are considered to be suitable alkaline feedstock for carbon mineralization. The aqueous carbon mineralization process of steelmaking slags generally includes the extraction of alkali earth metals in a low pH condition, followed by carbonation with CO_2 at a high pH. However, since steelmaking slags often exhibit limited leachability depending on their physicochemical properties, it often has an important role in the design of the carbon mineralization process. Here, the leachability of the steel slag was examined in both acidic and basic conditions. The extraction kinetics as well as the various operating factors, such as temperature, and particle size distribution, under an acidic condition were also examined for the potential carbon sequestration using the alkaline wastes.

Keywords: Carbon Dioxide, Carbon Mineralization, Steel Slag, Extraction, Industrial Waste

INTRODUCTION

Carbon mineralization processes can simultaneously store and utilize CO_2 captured from anthropogenic emission sources, such as a coal-fired power generation plant, and accordingly have attracted recent attention [1-3]. The carbon mineralization process involves spontaneous reactions between alkaline sources (e.g., Ca or Mg ions) and CO_2 to form solid carbonates which exhibit quite lower energy levels compared to atomic carbon (~178 kJ/mol) [4]. Numerous studies on carbon mineralization have adopted the aqueous pH swing process over multi-step methods. Generally, the pH swing process extracts alkali metal ions from naturally occurring or industrial feedstocks under low pH conditions using various acids (e.g., hydrochloric acid (HCl), nitric acid (HNO_3), sulfuric acid (H_2SO_4), acetic acid (CH_3COOH), and ethylenediaminetetraacetic acid (EDTA, $C_{10}H_{16}N_2O_8$) [5,6]. The metal ions precipitate with CO_2 in the elevated pH conditions, forming solid carbonates [7,8]. As feedstock for the alkali metals, either natural silicate minerals (e.g., wollastonite, olivine, serpentine) [9,10], or industrial wastes (e.g., steelmaking slags, coal ashes, and mining wastes) [2,11], can be considered as a feedstock. Moreover, industrial wastes hold particular benefits [12]: (i) Since industrial wastes exhibit a higher reactivity than natural minerals, they can significantly reduce operating costs for pre-treatment processes, as well as the use of extraction solvents. (ii) Industrial sources often make it possible to reduce the transportation cost of both CO_2 and alkali metal feedstocks for the carbonation process, because the industrial sectors which produce steelmaking slags and coal ashes also discharge large amounts of CO_2. And (iii), the industrial wastes often contain not only a considerable amount of alkali metals but also other valuable elements (e.g., Si, Fe, Al, or rare earth elements), which may be concentrated and recovered during pH swing-induced precipitation.

Since global steel production is expected to continue growing for the foreseeable future, it will be generating a huge amount of steelmaking slags [13]. The current management options for steelmaking slags are either disposal via landfills, or recycling as a granular base or as an aggregate material for construction applications. However, these simple uses can result in the leaching of hazardous metal elements from reclaimed slags, causing environmental issues. In contrast, since hazardous metal elements can be eliminated by the carbon mineralization process, steelmaking slags would have more plausible options for disposal or recycling. The carbon footprint of the steelmaking industry can also be lowered [14].

Steelmaking slags have various physicochemical properties depending on the types of ore and process. They generally contain a considerable amount of Ca and/or Mg. As a result, they have the potential to sequester 6-45% of the CO_2 generated by the steelmaking industry [11]. For this reason, steelmaking slags have recently

†To whom correspondence should be addressed.
E-mail: young@gist.ac.kr

been considered a promising storage medium for CO_2. Motivated by the above advantages, studies have reported on various carbon mineralization processes, integrated with extraction and carbonation steps [15,16]. Note that the steelmaking industry uses a variety of ores/coals and process conditions; thus, steelmaking slags exhibit distinct compositional and structural properties, which often has an important role in the design of the pH swing process.

Herein, we investigated the leaching behavior of elements in the steel slag under basic and acidic conditions. Since steel slag often exhibits basicity, because of its elemental composition, direct extraction with strong acids can lead to large increases in pH during the acidic elemental extraction. Accordingly, the leachability of the major elements in the steel slag in deionized water was examined. The reaction kinetics of the steel slag under acidic conditions, including reaction rate-limiting region, and activation energy, was calculated. The particle size distribution and their effects on the elemental extraction were also examined.

MATERIAL AND METHODS

1. Materials

Steel slag was supplied by a Korean steelmaking company. To examine the elemental leaching behavior of the steel slag, deionized water and HNO_3 (70%, Sigma Aldrich, Inc., USA) were used. The deionized water was obtained from a water purification system (HIQ-I, Coretech Co., Ltd., Republic of Korea).

2. Elemental Extraction of Steel Slag

The elemental extraction behavior of the steel slag was investigated in a batch reactor system. The particle size of the steel slag was controlled to between 54 and 200 μm. For the deionized water extraction, the raw steel slag was dissolved in deionized water (500 ml). The solid to liquid ratio (S/L ratio, kg/l) was adjusted to 1 : 20, 1 : 5, or 1 : 3. The extraction was performed while stirring at 300 rpm for 30 min. The temperature was maintained at 25 °C. After the reaction, the leachate was filtered using 0.2 μm filter paper and dried at 70 °C in a convection oven (OF-02GW, Jeio Tech Co., Ltd., Republic of Korea) for 24 h.

For the HNO_3 leaching, the elemental extraction kinetics of the steel slag was examined in 300 ml of 0.001 M HNO_3 solution. Since elemental extraction is affected by ligand type, as well as re-precipitation induced by dissociation into hydrated protons, the solution pH was maintained for approximately 3 for 2 h to minimize these effects. Reaction temperature was set to 25, 30, and 40 °C with a 1/1,000 of S/L ratio, and stirring rate was 700 rpm to minimize the limitation of mass transfer. During the extraction, the solution pH was measured using a pH meter (S220, Mettler-Toledo International Inc., USA), and slurry samples were extracted thirteen times, separated by a 0.2 μm syringe filter.

To investigate the effect of the particle size distribution on the elemental extraction, raw steel slag powder was sieved and then particle size (d_p) was controlled to d_p<150 μm, 150 μm<d_p<300 μm, 300 μm<d_p<600 μm, and d_p>600 μm. The S/L ratio was set to 1 : 20, and 50 ml of 1 M HNO_3 was used. The extraction was conducted for 2 h at 25 °C with a stirring rate of 300 rpm. After the extraction, filtration was conducted and then the residues were dried in a convection oven at 70 °C for 24 h.

3. Characterization of Steel Slag and Extraction Residue

The composition of the raw steel slag was analyzed using X-ray fluorescence (XRF, Axios FAST, PANalytical B.V., Netherlands). The crystalline structure of the raw steel slag was analyzed using powder X-ray diffractometer (PXRD, D8 Advance, Bruker Co., Germany). To characterize the mineralogical structure in the steel slag, the PXRD pattern was obtained in the 2θ range of 10-70° with a step size of 0.02°, using CuKα radiation (λ=1.5406 Å) with a generator voltage of 40 kV and a generator current of 40 mA. A particle size analyzer (PSA, LA-960, HORIBA Instruments, Inc., France) and the Brunauer-Emmett-Teller method (BET method, Nova Win BET Analyzer, Quantachrome Instruments Co., USA) were used to explore the particle size distribution, specific surface area and pore size, respectively. Scanning electron microscopy (SEM, S-4700 EMAX System, Hitachi, Ltd., Japan) was employed to identify the morphology of the solid residue after extraction. The elemental extraction behavior was investigated using inductively coupled plasma - optical emission spectroscopy (ICP-OES, OPTIMA 4300DV, PerkinElmer, Inc., USA). All leachate samples after extraction were diluted using 2 wt% HNO_3 for the ICP-OES analysis. The elemental extraction efficiency was calculated using Eq. (1):

$$\text{Extraction Efficiency (wt\%)} = \frac{W_l}{W_i} \times 100(\%) \quad (1)$$

where W_i and W_l indicate the initial mass of each element in the raw steel slag, and the extracted mass of the element in the leachate, respectively.

RESULTS AND DISCUSSION

1. Elemental Extraction of Steel Slag by Using Deionized Water

The major elements in the steel slag were analyzed using XRF. The average values of the powdered steel slag are given in Table 1. Steel slag contains Ca (~20 wt%) and Fe (~17 wt%) as major elements, and other elements such as Si (~8 wt%), Al (~5 wt%), and Mg (~3 wt%) were observed. To investigate the crystalline structure of each element, PXRD was employed, and the results are shown in Fig. 1. It was revealed that the steel slag used in this study contained a melilite group, specifically including gehlenite ($Ca_2Al[AlSiO_7]$, $P\bar{4}2_1m$), and åkermanite ($Ca_2Mg[Si_2O_7]$, $P\bar{4}2_1m$). Other calcium silicate minerals such as larnite (Ca_2SiO_4, $P2_1/n$), and kirschsteinite ($CaFeSiO_4$, *Pbnm*) were also observed. Note that melilite is one of the well-known crystalline structures in typical steel slags [17]. The broadened background pattern observed in the low 2θ region also indicates that amorphous phase silicon oxide (SiO_2) was included.

In general, steelmaking slags that exhibit a higher reactivity than

Table 1. Elemental compositions of steel slag analyzed by XRF (unit: wt%)

Ca	Mg	Fe	Al	Si	Mn	others
20.6±1.0	3.6±0.0	17.4±0.7	5.5±0.4	8.2±0.3	5.5±0.5	39.2±0.1

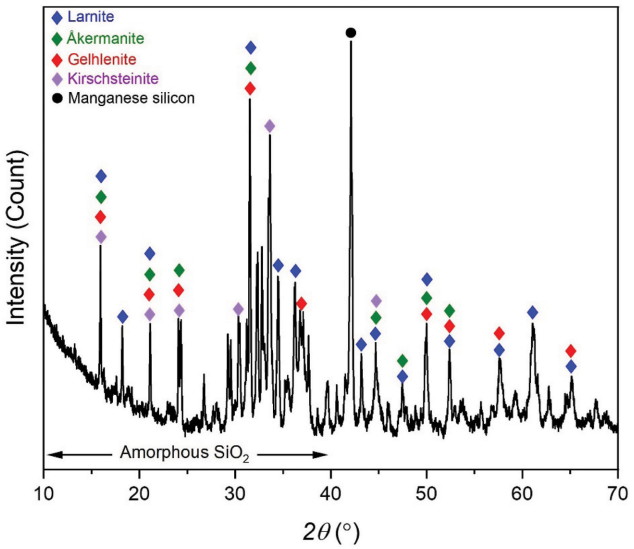

Fig. 1. Powder X-ray diffraction pattern of raw steel slag.

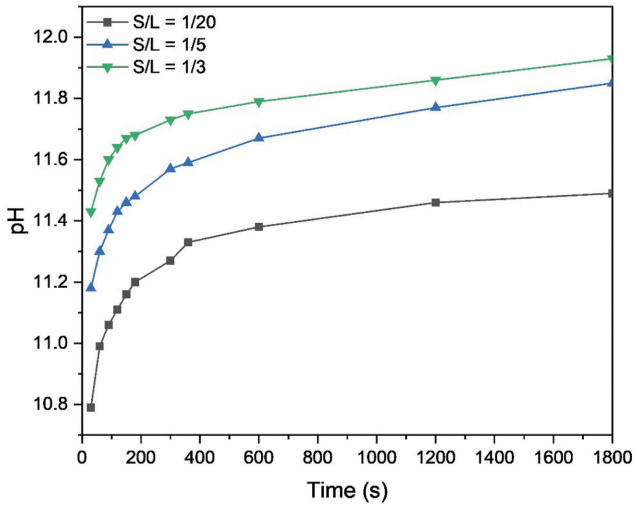

Fig. 2. pH variation depending on solid/liquid ratio as a function of time. The initial pH of deionized water was between 5 and 6.

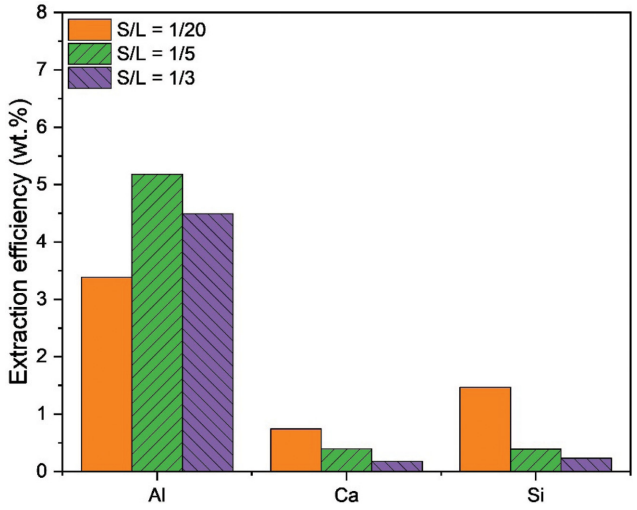

Fig. 3. Leaching efficiencies of aluminum (Al), calcium (Ca), and silicon (Si) from steel slag in deionized water.

natural minerals are alkaline in water due to the dissolution of alkali metals such as Ca and Mg. Thus, in order to examine the reactivity of the raw steel slag, elemental leaching was performed using deionized water in the batch reactor system at room temperature for 30 min. After the deionized water leaching with S/L=1/3, a solid residue was obtained. Then their particle properties measured by the BET method were compared with that of the raw steel slag (Table 2). The raw steel slag exhibited a surface area and pore volume of 1.861 m^2/g and 0.008 mL/g, respectively [18]. After leaching, the specific surface area of the steel slag was significantly larger (4.295 m^2/g) than that of the pristine steel slag. The pore volume also increased, from 0.008 to 0.015 ml/g. The changes in surface area and pore volume indicate that some amounts of elements in the raw steel slag were extracted by simply using deionized water. Note that slag basicity is determined by the weight ratios of calcium oxide (CaO) and magnesium oxide (MgO) divided by SiO_2 [19]. The elemental composition of the raw steel slag included ~20 wt% of Ca and Mg, with ~8 wt% of Si.

The basicity of the steel slag used in this experiment was examined via deionized water extraction with different S/L ratio. As shown in Fig. 2, the solution pH rapidly increased from neutral after the leaching and reached about pH 11-12. For the S/L ratios of 1/20, 1/5, and 1/3, the final solution pH reached ~11.4, 11.7, and 11.9, respectively. The initial pH of the deionized water was between 5 and 6.

Fig. 3 shows the elemental extraction efficiency of Al, Ca, and Si by deionized water in 30 min. The results show that Al had the highest extraction efficiency compared with Ca and Si. For Ca and Si, the extraction efficiency increased as the S/L ratio decreased. On the other hand, S/L=1/5 showed the highest extraction efficiency for Al. The extraction efficiency of Al was higher than that of Ca or Si because, in general, the Al-O bond is weaker than the bonds of Ca-O or Si-O; for example, the bonding energies for Al-O, Ca-O, and Si-O are 74.8, 346.6, 103.5 eV, respectively [20-23].

The re-precipitation behavior of Ca and Si also significantly influences extraction efficiency. For example, above pH 11 Ca ion prefers to form a solid calcium hydroxide ($Ca(OH)_2$) due to the thermodynamic stability, and thus, the concentration of Ca ions deceased as the solution pH increased. The re-precipitation of Ca and Si, and the formation of aluminum hydroxide ions ($Al(OH)_4^-$) in the

Table 2. Particle properties of steel slag analyzed by BET method

	Surface area (m^2/g)	Pore volume (mL/g)
Raw steel slag	1.861	0.008
Steel slag after deionized water extraction	4.295	0.015

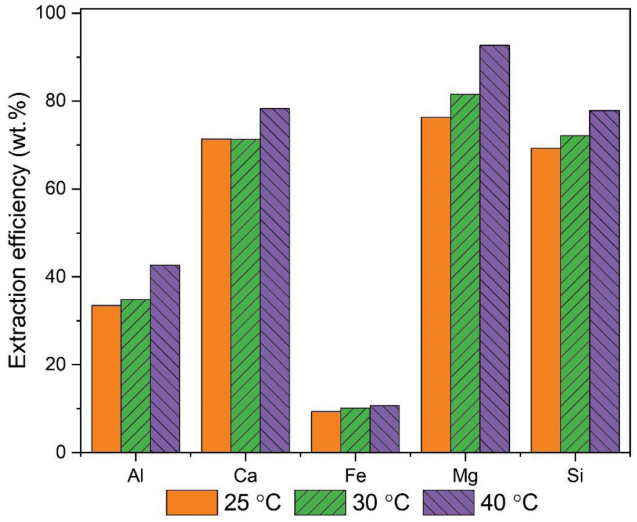

Fig. 4. Elemental extraction efficiency of steel slag in presence of HNO_3 for 2 h at 25, 30 and 40 °C.

basic condition can be explained by Eqs. (2) to (5) [20,24]:

$$CaO+SiO_2+3H_2O \leftrightarrow Ca(OH)_2+Si(OH)_4 \quad (2)$$

$$Si(OH)_4 \leftrightarrow H^+ + H_3SiO_4^- \quad (3)$$

$$2H_3SiO_4^- + Ca^{2+} \leftrightarrow H_6CaSi_2O_8 \quad (4)$$

$$Al(OH)_3+H_2O \leftrightarrow H^+ + Al(OH)_4^- \quad (5)$$

2. Extraction Kinetics of Steel Slag by Using HNO_3

The elemental extraction kinetics of the steel slag in the presence of HNO_3 was examined at approximately pH 3 for 2 h. The particle size of the steel slag was controlled between 54 and 200 μm. The elemental extraction of the steel slag in presence of HNO_3 is described below:

$MO+2HNO_3=M(NO_3)_2$
$+H_2O$ (M=divalent cations such as Ca^{2+}, and Mg^{2+})
$M_2O_3+6HNO_3=2M(NO_3)_3$
$+3H_2O$ (M=trivalent cations such as Al^{3+}, and Fe^{3+})

As shown in Fig. 4, increasing the reaction temperature from 25 to 40 °C enhanced the extraction efficiency of all elements, but the extent of the extraction enhancement depended on the types of element. Although the concentration of Fe was relatively high in the pristine steel slag (~17 wt%), the Fe extraction efficiency (9.4-10.7 wt%) was lower than that of other elements (32.5-92.7 wt%). To evaluate the reaction kinetics and rate-limiting step of the steel slag in the presence of HNO_3, the shrink-core model with a shrinking particle was adopted [20,25]. This model describes the reaction between a solid and a surrounding fluid, which consists of a surface chemical reaction, film layer diffusion, and product layer diffusion as the reaction rate-limiting regions. These equations are briefly described below:

$k_r t=t/\tau_r=1-(1-X)^{1/3}$ at surface chemical reaction
$k_d t=t/\tau_d=1-2/3X-(1-X)^{2/3}$ at film layer diffusion
$k_d t=t/\tau_d=1-3(1-X)^{2/3}+2(1-X)$ at product layer diffusion

where k_r and k_d are reaction rate constants (min^{-1}) in the chemical reaction and diffusion, respectively. τ_r and τ_d are the characteristic times for the chemical reaction and diffusion, respectively. X is the conversion ratio of a slag particle, and t is the reaction time (min). The extraction patterns for Al, Ca, Mg, Si, and Fe were plotted with the three reaction rate-limiting regions. All of the elements showed the highest linearity ($R_{Mg}^2 \geq 0.97$, $R_{Si}^2 \geq 0.98$, $R_{Ca}^2 \geq 0.99$, $R_{Al}^2 \geq 0.94$, and $R_{Fe}^2 \geq 0.97$) for product layer diffusion. The elemental extraction plots for product layer diffusion are described in Fig. 5. It suggests that the elemental extraction of steel slag in the presence of HNO_3 was limited by the diffusion of the product layer. As the temperature increased, faster reaction rate constants were observed. Reaction rate constants depending on reaction temperature were then calculated using the Arrhenius equation, as below [26]:

$$\ln k_d=(-E_a/R)(1/T)+\ln A$$

where E_a is the activation energy (kJ/mol), R is the universal gas constant (8.314 J/K·mol), A is the constant in each reaction, and T is the reaction temperature (K). Fig. 6 shows the Arrhenius plots of the elements extracted from the steel slag as a function of temperature. It was observed that the order of reaction kinetics, from fastest to slowest, was Mg, Si, Ca, Al, and Fe. The activation energy of Al, Ca, Mg, Fe, and Si was calculated to be 28.7, 15.7, 14.4, 37.5,

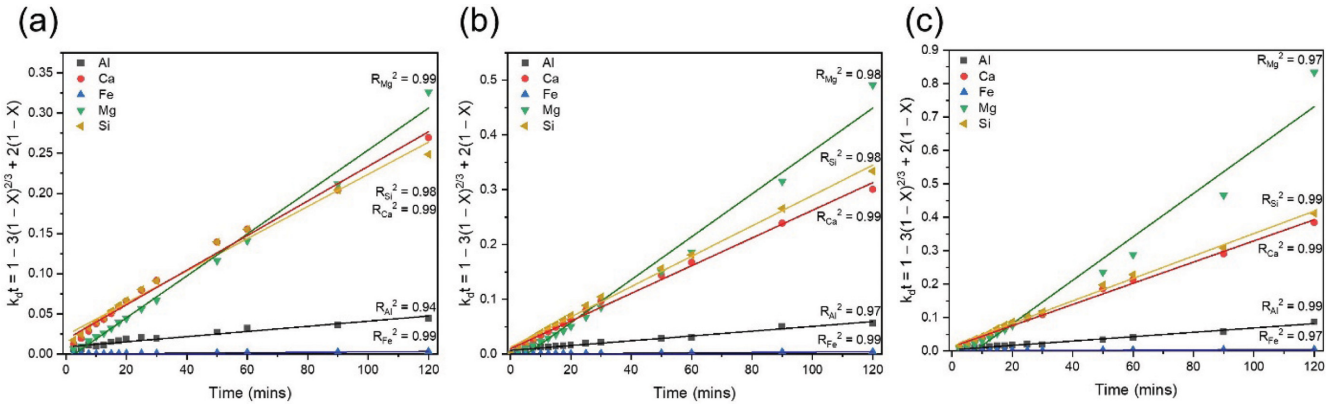

Fig. 5. Elemental extraction plots at (a) 25 °C, (b) 30 °C, and (c) 40 °C as a function of reaction time. The reaction rate-limiting region is set to the product layer diffusion.

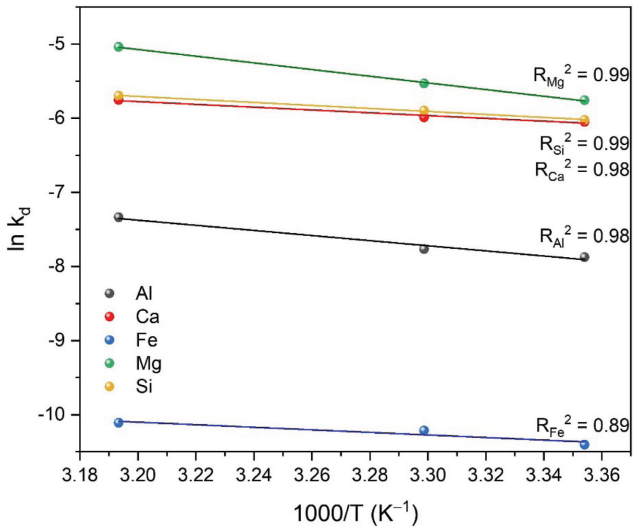

Fig. 6. Arrhenius plots for the major elements in steel slag; k_d indicates the reaction rate constant at the product layer diffusion.

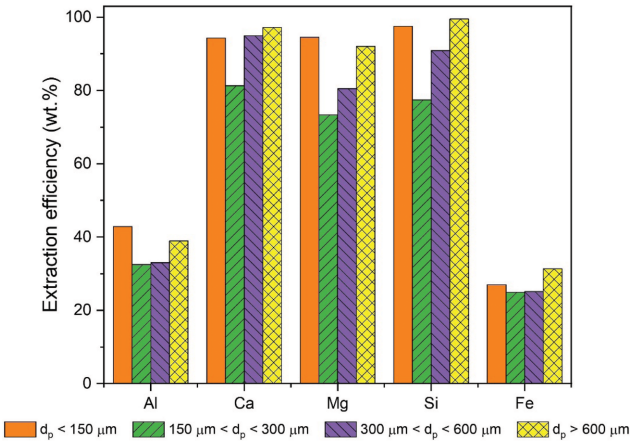

Fig. 7. Effect of particle size on elemental leaching efficiency of steel slag in HNO_3 solvent with an initial pH of 0.065.

and 16.9 kJ/mol, respectively. This suggests that Fe has the slowest extraction kinetics and lowest efficiency, induced by the highest activation energy, which was also related to the binding energy. Note that the binding energy of iron oxide (FeO) is 709 eV, whereas the binding energy of CaO is 346.6 eV [22,27].

3. Elemental Extraction of Size-controlled Steel Slag

The elemental extraction efficiency of the steel slag was investigated using size-controlled raw slag. 1 M HNO_3 solvent, set to an

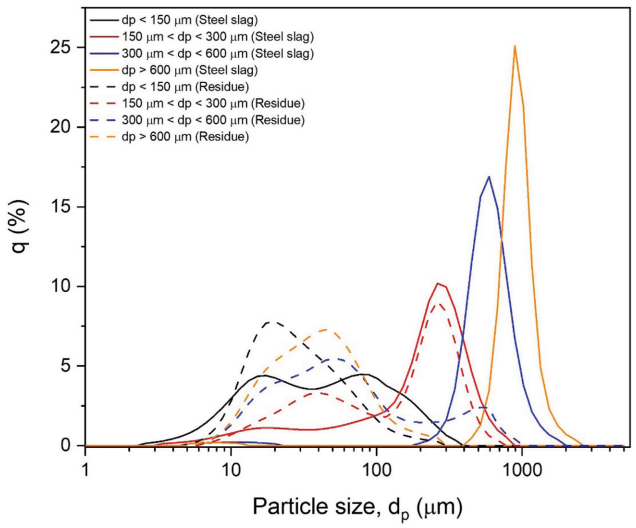

Fig. 8. Particle size distributions of the size-controlled steel slag. Solid and dash lines are the raw steel slag (Steel slag) and HNO_3 treated steel slag (Residue), respectively.

initial pH of 0.065, was used for extraction, and the S/L ratio was fixed at 1/20. Fig. 7 exhibits the extraction efficiency of the major elements depending on the particle size distribution, which was controlled to d_p<150 μm, 150 μm<d_p<300 μm, 300 μm<d_p<600 μm, and d_p>600 μm. For each particle size distribution, the particle mean sizes were 62.3, 221.5, 553, and 870.7 μm, respectively. After extraction, the mean sizes of the particles had changed to 34.8, 166.7, 116.7, and 46 μm, respectively (Table 3).

As shown in Fig. 7, the elemental extraction efficiency for Ca (~97 wt%), Mg (~92 wt%), and Si (~99 wt%) was higher than that of Fe (~31 wt%), and Al (~39 wt%), respectively, for all particle distributions. It is believed that the low extraction of Fe is related to its high activation energy (37.5 kJ/mol), as well as specific elemental distributions on the particle surface. Hong et al., previously performed steel slag extraction using HNO_3 in a differential-bed reactor system, and it was observed that the steel slag had a lower Fe extraction efficiency than Ca and Mg, even though the steel slag contained a considerable amount of Fe [18]. Like the previous differential-bed reactor experiment, the current work conducted in a batch reactor system showed a relatively lower extraction efficiency for Fe.

Table 3 shows the particle size and solution pH of the steel slag before and after HNO_3 extraction. The solution pH slightly increased after extraction to ~0.5, but the differences among the cases were not significant. On the other hand, the mean particle size sig-

Table 3. Particle size of steel slag and solution pH before and after HNO_3 extraction

Particle distribution (μm)	pH (before extraction)	Mean size (before extraction, μm)	pH (after extraction)	Mean size (after extraction, μm)
d_p<150	0.065	62.3	0.539	34.8
150<d_p<300	0.065	221.5	0.425	166.7
300<d_p<600	0.065	553	0.495	116.7
d_p>600	0.065	870.7	0.513	46

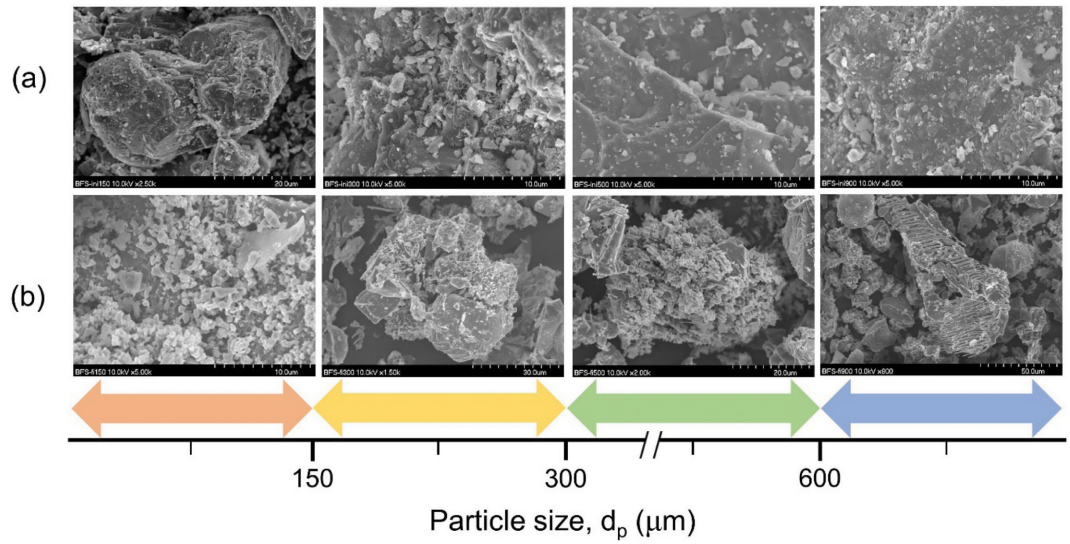

Fig. 9. SEM images of (a) raw steel slag and (b) steel slag after HNO_3 solvent extraction.

nificantly decreased after extraction. As the particle size became smaller, the elemental extraction efficiency increased, due to the evolution of a larger surface area [28]. The elemental extraction efficiency of large particles (i.e., 300 μm<d_p<600 μm, and d_p>600 μm) was higher than small particles (150 μm<d_p<300 μm), and this was attributed to the change in particle size distribution rather than pH in the extraction step.

Fig. 8 shows the change in particle size distribution before and after HNO_3 extraction. Large particles could be more easily crushed than small particles, due to the difference in surface energy per unit area [29]. Thus, the larger the particle size, the greater the change in particle size after extraction. This indicates that larger slag particles collide with each other during extraction, and since crushed particles have a larger surface area, it improves the extraction efficiency of all elements. Fig. 9 shows the morphology of the raw steel slag and the solid residues after HNO_3 extraction. The particles in the raw steel slag had an even surface, but the extracted slag showed pores growing on the particle surface. This is postulated to be caused by partial extraction on the particle surface, which at the same time enhances the effects of crushing and fragmentation as collisions occur between particles.

CONCLUSIONS

We investigated the elemental extraction behavior of steel slag in a batch reactor system using deionized water and HNO_3. Due to the intrinsic basicity of the steel slag, extraction using deionized water allowed the partial dissolution of Al, Ca, and Si with increasing pH, but other elements such as Fe were not extracted. As the extraction variables, particle size distribution and reaction temperature were considered in the acidic condition using HNO_3. It resulted in higher elemental extraction efficiency for Ca (~97 wt%), Mg (~92 wt%), and Si (~99 wt%), whereas other elements such as Fe (~31 wt%), and Al (~39 wt%), were not significantly extracted. This was attributed to the difference in elemental activation energy, controlled by the product layer diffusion. The results indicated that when steel slag is selected as the feedstock, the particle size could be flexibly adapted to enhance the extraction of elements under acidic condition during the carbon mineralization process. This study could contribute to designing an extraction process using alkaline wastes for carbon sequestration.

DECLARATION OF COMPETING INTEREST

The authors report no conflict of interest.

ACKNOWLEDGEMENT

This work was supported by "Human Resources Program in Energy Technology" of the Korea Institute of Energy Technology Evaluation and Planning (KETEP), granted financial resource from the Ministry of Trade, Industry & Energy, Republic of Korea. (No. 20194010000220).

REFERENCES

1. G. Gadikota, N*ature Rev. Chem*., **4**, 78 (2020).
2. R. Chang, S. Kim, S. Lee, S. Choi, M. Kim and Y. Park, *Front. Energy Res*., **5**, 17 (2017)
3. S. Moon, Y. Lee, S. Choi, S. Hong, S. Lee, A.-H. A. Park and Y. Park, *Org. Process Res. Dev*., **1723**, 22 (2018).
4. S. Hong, G. Sim, S. Moon and Y. Park, *Energy Fuels*, **3532**, 34 (2020).
5. H. Zhao, Y. Park, D. H. Lee and A.-H. A. Park, *Phys. Chem. Chem. Phys*., **15**, 15185 (2013).
6. S. Teir, H. Revitzer, S. Eloneva, C.-J. Fogelholm and R. Zevenhoven, *Int. J. Miner. Process*., **83**, 36 (2007).
7. X. Wang and M. Maroto-Valer, *Energy Procedia*, **4**, 4930 (2011).
8. S. Teir, S. Eloneva, C. J. Fogelholm and R. Zevenhoven, *Energy*, **32**, 528 (2007).
9. G. Rim, A. K. Marchese, P. Stallworth, S. G. Greenbaum and A.-H. A. Park, *Chem. Eng. J*., **396**, 125204 (2020).
10. A.-H. A. Park, R. Jadhav and L.-S. Fan, *Can. J. Chem. Eng*., **81**, 885

(2003).
11. S. N. Lekakh, D. G. C. Robertson, C. H. Rawlins, V. L. Richards and K. D. Peaslee, *Metall. Mater. Trans. B*, **39**, 484 (2008).
12. A. Sanna, M. Uibu, G. Caramanna, R. Kuusik and M. M. Maroto-Valer, *Chem. Soc. Rev.*, **43**, 8049 (2014).
13. World Steel Association, *World steel in figures*, Publications, Belgium (2020).
14. F. Engström, M. L. Larsson, C. Samuelsson, Å. Sandström, R. Robinson and B. Björkman, *Steel Res. Int.*, **85**, 607 (2014).
15. A.-H. A. Park and L.-S. Fan, *Chem. Eng. Sci.*, **59**, 5241 (2004).
16. A. Azdarpour, M. Asadullah, E. Mohammadian, H. Hamidi, R. Junin and M. A. Karaei, *Chem. Eng. J.*, **279**, 615 (2015).
17. S. E. Ashbrook and D. M. Dawson, *Nucl. Magn. Reson.*, **45**, 1 (2016).
18. S. Hong, H. D. Huang, G. Rim, Y. Park and A.-H. A. Park, *ACS Sustain. Chem. Eng.*, **8**(50), 18519 (2020).
19. S.-J. Kim, J. Takekawa, H. Shibata, S.-y. Kitamura and K. Yamaguchi, *ISIJ Int.*, **53**, 1715 (2013).
20. I. Nikolić, A. Drinčić, D. Djurović, L. Karanović, V. V. Radmilović and V. R. Radmilović, *Constr. Build. Mater.*, **108**, 1 (2016).
21. B. R. Strohmeier, *Surf. Interf. Anal.*, **15**, 51 (1990).
22. B. Demri and D. Muster, *J. Mater. Process. Technol.*, **55**, 311 (1995).
23. C. D. Wagner, D. E. Passoja, H. F. Hillery, T. G. Kinisky, H. A. Six, W. T. Jansen and J. A. Taylor, *J. Vacuum Sci. Technol.*, **21**, 933 (1982).
24. H. Maraghechi, F. Rajabipour, C. G. Pantano and W. D. Burgos, *Cem. Concr. Res.*, **87**, 1 (2016).
25. S.-Y. Pan, T.-C. Ling, A.-H. A. Park and P.-C. Chiang, *Aerosol Air Qual. Res.*, **18**, 829 (2018).
26. H. S. Fogler, *Elements of chemical reaction engineering*, Practice Hall, Publications, New Jersey (2004).
27. M. C. Biesinger, B. P. Payne, A. P. Grosvenor, L. W. M. Lau, A. R. Gerson and R. S. C. Smart, *Appl. Surf. Sci.*, **257**, 2717 (2011).
28. W. J. J. Huijgen, G.-J. Witkamp and R. N. J. Comans, *Environ. Sci. Technol.*, **39**, 9676 (2005).
29. W. L. McCabe, J. S. Smith and P. Harriott, *Unit operations of chemical engineering*, McGraw-Hill Education, Publication, New York (2004).